Dalton Transactions

PAPER

View Article Online
View Journal | View Issue

Cite this: *Dalton Trans.*, 2015, **44**, 11852

Syntheses, structures, photoluminescence and photocatalysis of chiral 3D Cd(II) frameworks from achiral mixed flexible ligands by spontaneous resolution†

Yan-Qiong Sun,*[a,b] Jie-Cen Zhong,[a] Ling Ding[a] and Yi-Ping Chen[a]

Received 17th April 2015,
Accepted 14th May 2015

DOI: 10.1039/c5dt01454a

www.rsc.org/dalton

Unprecedented two homochiral Cd(II) enantiomers $[Cd(dtba)(bpp)]_n$ (**1**: **1P** and **1M**) (H_2dtba = 2,2′-dithiodibenzoic acid, bpp = 1,3-bis(4-pyridyl)propane), were obtained by self-assembly with mixed achiral flexible ligands. Single-crystal X-ray diffraction analysis reveals that complexes **1P** and **1M** crystallize in trigonal space groups $P3_121$ and $P3_221$, respectively. The compounds are optically active, and their UV spectra in the solid state showed Cotton effects in the opposite directions. Compounds **1P** and **1M** present the examples of three-interpenetrating chiral frameworks with triangular and quasi-heart-like threefold helical chiral channels, chair-like twofold helical chiral channels and one type of threefold double-helical chain. The 3D metal–organic framework can be regarded as a *bcu*-type topology with the symbol of 8^6. The photoluminescent properties of compound **1** have been studied. Remarkably, compound **1** exhibits good photocatalytic activity for degradation of dyes under the simulated sunlight irradiation in the pH = 3 aqueous solution.

Introduction

Helical structures through self-assembly are necessary in our life and are of interest in recent research due to their novel chiral structures.[1,2] So the design and synthesis of chiral complexes are of particular interest owing to their potential applications in enantioselective separation[3,4] and asymmetric catalysis.[5,6] To the best of our knowledge, there are three methods to obtain chiral complexes: (1) stereoselective syntheses using enantiopure organic ligands.[7] With this method, the absolute configuration of the chiral complexes can be predetermined and the product crystals would be homochiral. (2) Chiral syntheses using chiral auxiliaries such as chiral solvents, catalysts or templates lead to a particular handedness.[8] (3) Spontaneous resolution upon crystallization without any chiral auxiliaries.[9,10] A spontaneous resolution phenomenon is observed for a certain kind of racemic mixed crystal comprising equal amounts of enantiomers with opposite chirality. A large number of examples of chiral spontaneous resolution have been reported.[11,12] However, so far, spontaneous resolution without any chiral auxiliaries has been hard to predict because the laws of physics determining the processes have not yet been fully understood. Therefore, it is difficult to control the spontaneous resolution process owing to the discriminative interactions influencing chirality resolution. Generally, chirally discriminative interactions may arise from coordination bonds, hydrogen bonds, or π–π packing interactions due to their strong, selective and direction natures. In most instances of spontaneous resolution, chirality results from the coordination of the achiral ligands with the metal ions to form helical chains running along the screw axis. The achiral organic ligands with flexible conformations and skew coordination orientations are favorable for constructing a helical structure.

Along these lines, we chose the long flexible ligands of 2,2′-dithiodibenzoic acid (H_2dtba) and 1,3-bis(4-pyridyl)propane (bpp) to construct chiral coordination polymers based on the following consideration: (1) the twisted conformations of H_2dtba and bpp ligands provide the potential capability to form helical structures. The rotatable C–S and S–S single bonds in the H_2dtba ligand and C–C bonds in the bpp ligand enable the ligands to have flexible conformational adaptations (Fig. S1†).[13–15] (2) Their axial chirality potentially generates M and P enantiomers.[16] The flexible 1,3-bis(4-pyridyl)propane ligand (bpp) with a trimethylene part can provide a variety of

[a]*College of Chemistry, Fuzhou University, Fuzhou, Fujian 350108, People's Republic of China. E-mail: sunyq@fzu.edu.cn; Fax: +86-591-22866340*
[b]*State Key Laboratory of Structural Chemistry, Fujian Institute of Research on the Structure of Matter, Chinese Academy of Sciences, Fuzhou, Fujian 350002, PR China*
† Electronic supplementary information (ESI) available: Supplementary 14 plots including structures, luminescent spectra, XPRD, TG and FT-IR. CCDC 1012515 and 1012516. For ESI and crystallographic data in CIF or other electronic format see DOI: 10.1039/c5dt01454a

conformations (*TT*, *TG*, *GG* and *GG′*, where *T* = *trans* and *G* = *gauche*) (Fig. S2†), which display quite different N–N distances and bend angles.[17] (3) The skew coordination orientation of the carboxyl groups in the H_2dtba ligand is favorable for constructing a helical structure, which has been well documented in metal carboxylates.[18]

In this paper, we report two homochiral enantiomers of $[Cd(dtba)(bpp)]_n$ (**1P** and **1M**), which are resolved by spontaneous resolution upon crystallization, in the absence of any chiral sources into 3D chiral metal–organic frameworks. Compounds **1P** and **1M** consist of three-fold $[Cd(dtba)]_n$ single helical chains and three-fold $[Cd(bpp)]_n$ double helical chains. Interestingly, the helical chirality handedness can influence complexes **1P** and **1M** to induce $P3_1$ and $P3_2$ helical chains, respectively. Furthermore, the chiral compounds were characterized with solid-state circular dichroism (CD) spectra and fluorescence spectra. Compound **1** (**1P** and **1M**) is found to be able to photocatalytically degrade Rhodamine-B in a pH = 3 aqueous solution in a relatively efficient way.

Experimental section

General information

Commercially available solvents and chemicals were used without further purification. IR spectra were recorded using KBr pellets on a Perkin-Elmer Spectrum 2000 FT-IR in the range 400–4000 cm^{-1}. The powder XRD patterns were recorded on a PANalytical X'pert Pro diffractometer equipped with Co Kα radiation (λ = 1.78901 Å) at room temperature. The C, H and N elemental analyses were performed with an Elementar Vario EL III elemental analyzer. Thermogravimetric data were collected on a Mettler Toledo TGA/SDTA 851^e analyzer under flowing nitrogen at a heating rate of 10 °C min^{-1}. Luminescence measurements were made with an Edinburgh Instrument FS920 TCSPC luminescence spectrometer on powder crystal material of the compounds. CD spectra were recorded on a MOS-450 spectrophotometer, the scan rate was 500 nm min^{-1}, and all of the spectra were accumulated two times.

Photocatalytic activities of the prepared samples were evaluated by the degradation of RhB (10 mg L^{-1}) under simulated irradiation. A 300 W Xenon lamp was used as the light source. Before the irradiation, compound **1** as a photocatalyst was dispersed into the solution by magnetically stirring in the dark for about 2 h to reach an adsorption/desorption equilibrium between the photocatalyst and RhB. Then, the suspensions were exposed to simulated sunlight irradiation. About 3 mL of the suspension was sampled every 20 min and centrifuged to separate the photocatalyst. The filtrate was analyzed by using a UV-vis spectrophotometer (Shimadzu UV1750), and the concentration of RhB was monitored at 554 nm.

Synthesis of compounds

$[Cd(dtba)_{0.5}(bpp)_{0.5}]_n$. 2,2′-Dithiodibenzoic acid (0.090 g, 0.3 mmol), 1,3-bis(4-pyridyl)propane (0.040 g, 0.2 mmol) and CdO (0.025 g, 0.2 mmol) were dissolved in 5 ml DMF. After being stirred for 30 min, the aqueous solution was sealed in a 25 ml Parr Teflon-lined stainless steel auto-clave and heated at 80 °C for 2 d and then cooled to room temperature for 1 d. Brown block crystals suitable for X-ray analysis were obtained in 70% yield on cadmium basis. Anal. Calc. for $C_{27}H_{22}CdN_2O_4S_2$: C, 52.37; H, 3.61; N, 4.52 wt%; Found: C, 52.68; H, 3.58; N, 4.56 wt%. The IR data (KBr, cm^{-1}): 3060(w), 1650(s), 1573(s), 1458(s), 1398(s), 1282(m), 1036(m), 860(m), 746(s), 478(m) (Fig. S3†).

X-ray crystallography

X-ray single crystal diffraction data for complexes **1P** and **1M** were collected on a Bruker APEX II diffractometer at room temperature equipped with a fine focus, 2.0 kW sealed tube X-ray source (Mo Kα radiation, λ = 0.71073 Å) operating at 50 kV and 30 mA (λ = 0.71073 Å). The diffraction points of $I > 2\sigma(I)$ were selected to determine the structures of complexes **1P** and **1M**, and solved by direct methods and refined by full-matrix least-squares methods using the SHELXS and SHELXL programs of the crystallographic software package.[19] The structures of **1P** and **1M** were solved in trigonal chiral, enantiomorphic space groups $P3_121$ (space group no. 152) and $P3_221$ (space group no. 154) respectively, with correct configurations. All metal atoms, nitrogen, sulfur atoms, carbon and oxygen atoms in **1P** and **1M** were refined with anisotropic thermal parameters on F^2. All hydrogen atoms were generated geometrically (C–H 0.93 Å) and refined with isotropic thermal parameters riding on the parent atoms. The crystallographic data and structural refinement parameters for **1P** and **1M** are listed in Table 1. CCDC numbers: 1012515 for **1P** and 1012516 for **1M**.

Table 1 Crystal data and structure refinement for **1**

Compound	**1P**	**1M**
Formula	$C_{27}H_{22}CdN_2O_4S_2$	$C_{27}H_{22}CdN_2O_4S_2$
M_r (g mol^{-1})	614.99	614.99
Crystal system	Trigonal	Trigonal
Space group	$P3_121$	$P3_221$
a (Å)	11.5660(10)	11.684(4)
b (Å)	11.5660(10)	11.684(4)
c (Å)	16.035(3)	16.157(8)
α (°)	90	90
β (°)	90	90
γ (°)	120	120
V (Å^3)	1857.7(4)	1910.1(17)
Z	3	3
D_c (g cm^{-3})	1.649	1.608
μ (mm^{-1})	1.088	1.058
Flack parameter	0.15(2)	−0.02(3)
Reflns collected/unique	12 954/2224	18 332/2914
R_{int}	0.0523	0.1174
θ range/°	2.03–25.29	3.23–27.48
F(000)	936	935
GOOF on F^2	1.076	1.215
Final R indices[a] [$I > 2\sigma(I)$]	R_1 = 0.0924, wR_2 = 0.1986	R_1 = 0.1288, wR_2 = 0.1843
R indices (all data)	R_1 = 0.0993, wR_2 = 0.2033	R_1 = 0.1850, wR_2 = 0.2049

[a] $R_1 = \sum||F_o| - |F_c||/\sum|F_o|$. $wR_2 = \{\sum[w(F_o^2 - F_c)^2]/\sum[w(F_o^2)^2]\}^{1/2}$.

Photocatalytic experiment

The typical process was presented as follows: 20 mg of compound **1** was mixed together with 25 mL of 10 mg L^{-1} (C_0) RhB solution in a beaker by stirring for 2 h, which makes it to reach the surface-adsorption equilibrium on the particles of compound **1**. Then the mixture was stirred continuously under simulated sunlight irradiation from a 300 W high pressure Xe lamp. At 0, 20, 40, 60, 80, 100 and 120 min 3 mL of the sample was taken out of the beaker, respectively, then followed by several centrifugations to remove compound **1**, and a clear solution was obtained for UV–vis analysis.

Results and discussion

Crystal structure

Single crystal X-ray analysis reveals that complexes of $[Cd(dtba)(bpp)]_n$ (**1P** and **1M**) crystallize in the trigonal enantiomeric space group $P3_121$ or $P3_221$ with a flack parameter of 0.15(2) or −0.02(3), respectively, indicating enantiomeric purity of the single crystals despite the use of achiral reagents. The structures of compounds **1P** and **1M** are enantiomorphs. The asymmetric units of both **1P** and **1M** contain half of the Cd^{2+} ion, half of the $dtba^{2-}$ ligand and half of the bpp ligand. The six-coordinated Cd center lies in the two-fold axis and is coordinated by four carboxylic oxygen atoms of two dtba ligands and two nitrogen atoms from two bpp ligands (Fig. 1) in a distorted octahedron form. The lengths of Cd–O and Cd–N are in the range of 2.216(6)–2.43(3) Å and 2.283(18)–2.36(2) Å, respectively. The $dtba^{2-}$ ligand, with a two-fold axis passing through the middle of the S–S bond, adopts a twist conformation with a C–S–S–C torsion angle of *ca.* 86°, which shows the axial chirality with the M- and P-forms of the enantiomers for constructing interesting coordination frameworks. All the carboxylate groups of the $dtba^{2-}$ ligand adopt chelating modes to connect two Cd(II) atoms (Fig. S4†). The bpp molecule, with a two-fold axis passing through the C8 atom, has *TT* configuration and bridges two Cd(II) centers (Fig. S5†).

The most interesting structural features of compounds **1P** and **1M** are the linkage between the Cd^{2+} centres and the two long flexible ligands, H_2dtba and bpp to form an unprecedented three-dimensional framework with two types of three-fold helical chiral channels, three types of twofold helical chiral channels and one type of threefold double-helical chain. There are triangular and quasi-heart-like threefold helical chiral channels in **1P** and **1M** compounds. The triangular helical channels (right-handed in **1P**, left-handed in **1M**) are made of [Cd(dtba)] single helical chains formed by the carboxylate group of $dtba^{2-}$ ligands bridging Cd(II) atoms with a pitch of 16.274(2) Å (Fig. 2a). The [Cd(dtba)] single helical chains wind around a threefold screw axis running parallel to the *c* axis to form a right-handed helical channel in **1P** or a left-handed helical channel in **1M** with a triangular shape (dimensions 10.68 × 10.68 × 10.68 Å) (Fig. 2b). The quasi-heart-like threefold helical channels (right-handed in **1P**, left-handed helices in **1M**) consist of three repeating Cd-dtba–Cd-bpp linkages, in which the Cd atoms are alternatively bridged by $dtba^{2-}$ and bpp ligands with a pitch of 16.274(2) Å (Fig. 3). In addition, there are similar chair-like twofold helical chiral channels with a reverse helical orientation to threefold helical chiral channels (left-handed helices in **1P**, right-handed helices in **1M**) running parallel to the [100], [010] and [110] directions, respectively (Fig. 4). The three types of chair-like helical channels are all constructed from the triple-helical chains. The separations between the adjacent helical chains are the same as the length of the *a* or *b* axis (11.730(1) Å). The pitch of the chair-like helical channels are three times the length of *a* or *b* axis. The triple-helical chains are made of two repeating Cd-dtba–Cd-bpp linkages running parallel to the twofold screw axes.

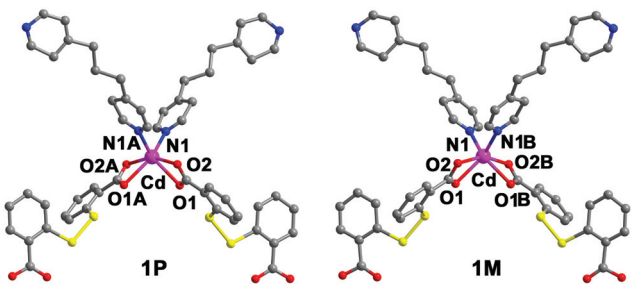

Fig. 1 The coordination environments of Cd^{2+} in **1P** and **1M**. Atoms having "A", or "B" in their labels are symmetry-generated. A: 1 + *x* − *y*, −*y* + 2, 2/3 − *z*; B: *y*, *x*, −*z*+. Hydrogen atoms are omitted for clarity. Color code: Cd, purple; O, red; N, blue; C, grey; S, yellow.

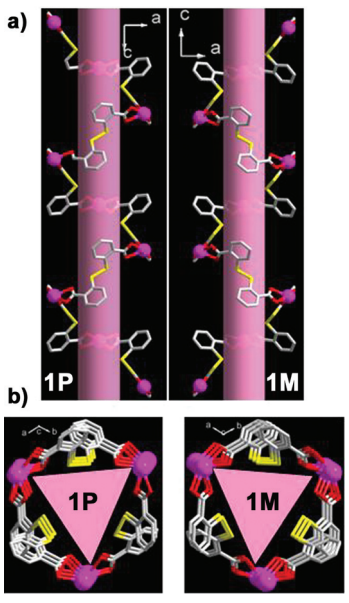

Fig. 2 (a) View of the [Cd(dtba)] threefold helices (right-handed in **1P**, left-handed in **1M**) running along the *c* axis; (b) view of the triangular helical channels containing [Cd(dtba)] threefold helices in **1P** and **1M** along the *c*-axis.

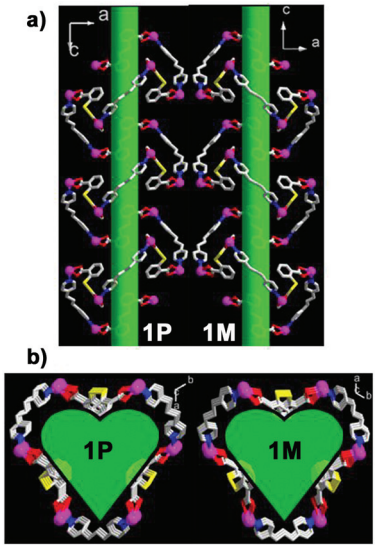

Fig. 3 (a) View of the [Cd_2(dtba)(bpp)] threefold helices (right-handed in **1P**, left-handed in **1M**) running along the *c* axis; (b) view of the quasi-heart-like helical channels containing [Cd_2(dtba)(bpp)] threefold helices in **1P** and **1M** along the *c*-axis.

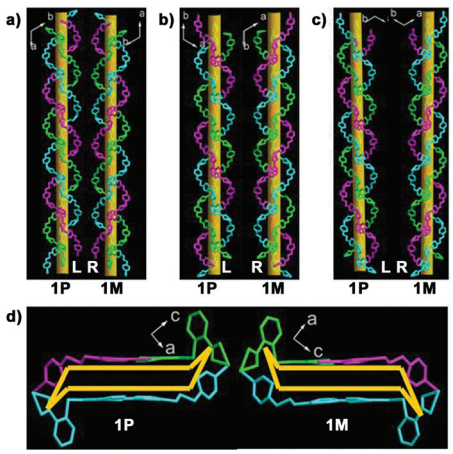

Fig. 4 View of the chair-like channels constructed from the two-fold triple-helical chains (left-handed (L) in **1P**, right-handed (R) in **1M**) running along the [100] direction (a), [010] direction (b) and [110] direction (c). The triple-helical chains are marked with purple, green and cyan. (d) View of the chair-like channels along the *b* axis.

Remarkably, bpp ligands with the *TT* configuration bridge Cd^{2+} centres to form two equivalent Cd-bpp helical chains with the same helical orientation as the chair-like twofold helical channels (left-handed helices in **1P**, right-handed helices in **1M**) with the pitch twice as the length of the *c* axis running along the threefold screw axis. The separation between the two equivalent Cd-bpp helical chains is the same as the length of the *c* axis (Fig. 5). The two equivalent Cd-bpp helical chains strand spiral parallel around a threefold screw axis to generate double-helical chains. The double-helical

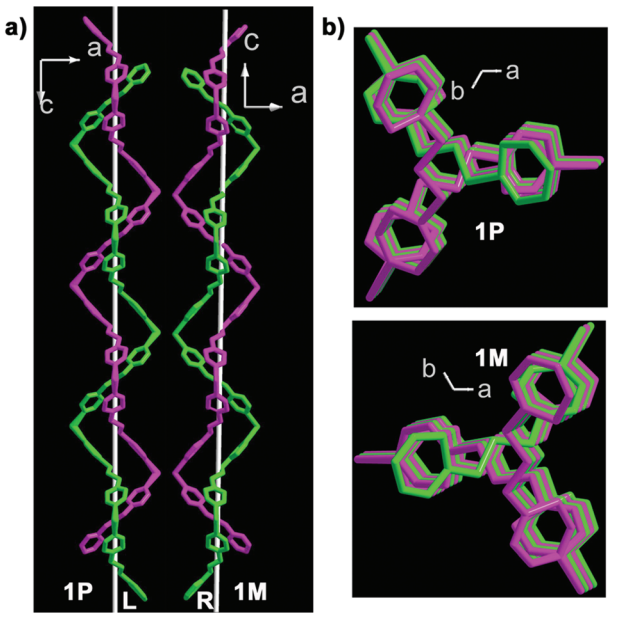

Fig. 5 (a) The threefold [Cd(bpp)]$_n$ double-stranded helices (left-handed (L) in **1P**, right-handed (R) in **1M**) viewed upright to the *c* axis. The double helical chains are marked with purple, and green. (b) View of the threefold double-stranded helices along the *c* axis.

chains overlap and look like flowers with three petals as viewed from the *c* axis. The double-helical chains as pillars are connected by the $dtba^{2-}$ ligands *via* Cd–O interactions to produce a 3D open-framework, exhibiting different helical chiral channels (Fig. 6a and b). The large porosity of **1P** and **1M** allows the interpenetration of the network by other independent networks. In **1P** and **1M**, there are three interpenetrated nets, which are related to the translation vector of *a*

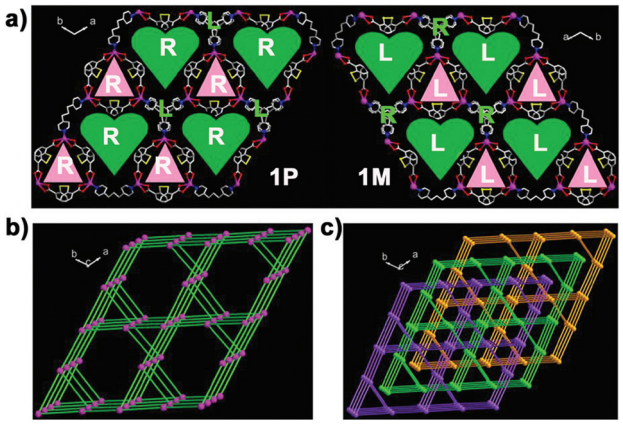

Fig. 6 (a) The 3D frameworks of **1P** and **1M** viewed along the *c* axis, showing triangular and quasi-heart-like threefold helical chiral channels in **1P** and **1M** and double-helical chains. L and R indicate the left- and right-handed helical channels; (b) a single 8^6 network in **1P** viewed close along the *c* axis. (c) Three interpenetrating 8^6 nets (purple, green and orange) in **1P** viewed along the *c* axis.

(11.730(1) Å), so **1P** and **1M** are threefold interpenetrated 3D chiral frameworks (Fig. 6c).

Topologically, the 3D metal–organic framework of **1** can be regarded as a uninodal four-connected *bcu*-topology net taking the Cd^{2+} ions as four-connected nodes. The Schäfli symbol for the four-connected uniform networked is 8^6, which is calculated using TOPOS 4.0 (Fig. 6b). The extended point symbol is $[8^6{\cdot}8^6{\cdot}8^7{\cdot}8^7{\cdot}8^7{\cdot}8^7]$. Interestingly, compounds **1P** and **1M** crystallize in the chiral space $P3_121$ (no. 152) or $P3_221$ (no. 154). Therefore, compounds **1P** and **1M** show a chiral threefold interpenetrating 4-connected 8^6 network, which is rarely reported.

XRD, IR spectra and UV spectral analyses

As shown in Fig. S6,† the good agreement of experimental XRD patterns with the simulated patterns indicates phase purity of compound **1**.

The IR spectrum (Fig. S3†) of **1** exhibits strong and sharp absorption peaks at 1573 and 1398 cm^{-1} associated with the ν_{asym}(C═O) and ν_{sym}(C═O), respectively, and also peaks at 860 and 746 cm^{-1} corresponding to the ν_s(S–S) of the $dtba^{2-}$ ligand.

The UV-vis absorption spectrum was recorded at room temperature for **1**. Absorption data *R*/*S* (*R*, absorption coefficient; *S*, scattering factor) were calculated from the reflectance data using the Kubelka–Munk function. The optical band gap of 2.92 eV (point a in Fig. S7†) was measured as the intersection point between the energy axis at the absorption offset and the line extrapolated from the sharp absorption edge in the K–M *versus* *E* (eV) plot.[20] The optical band gap indicates that compound **1** is a semiconducting MOF, underlining its potential as a photocatalyst.

The chiroptical characteristics of compound 1 by CD spectra

Circular dichroism (CD) spectroscopy is the most common technique for characterizing the optical activity of chiral materials. In order to confirm the compounds **1P** and **1M** enantiomeric nature, individual crystals were characterized by solid-state circular dichroism (CD) spectroscopy in KCl pellets (Fig. 7). As shown in Fig. 7, the CD spectra of enantiomers are nearly mirror images of each other, indicating the enantiomeric nature of the compounds. The signals of the purple curve (**1P**) and the orange curve (**1M**) can be observed with the obvious Cotton effect. The purple curve showed three positive peaks at 220 nm, 267 nm and 317 nm, as well as one negative peak at 243 nm, which may be considered as the signature of the **1P** helicity. However, opposite signals at the same wavelengths for compound **1** are observed too, showing only one strong positive peak at 247 nm, and two negative peaks at 221 nm and 320 nm corresponding to **1M**. There is no dichroism signal in a mixture of a few crystals. Concurrence of the CD experiments and single-crystal studies confirms that the sample is a conglomerate consisting of enantiomorphs **1P** and **1M**, which confirms spontaneous resolution during the course of crystallization.

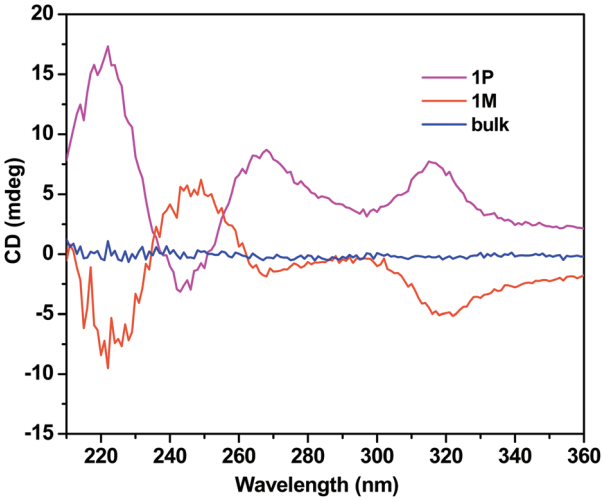

Fig. 7 Solid-state CD spectra of **1P** (purple), an enantiomorphic **1M** (red), and a mixture of a few crystals (blue).

Thermal properties

Thermal analysis was carried out from 30 °C to 1000 for **1** under a nitrogen atmosphere (Fig. S8†). Because there are no solvent molecules in **1**, compound **1** is stable up to 280 °C; the first weight loss of 50.68% (calcd, 49.82%) in the temperature range of 280–370 °C can be assigned to the decomposition of the $dtba^{2-}$ ligand. The second weight loss of 16.93% (calcd, 16.12%) in the range of 370–470 °C corresponds to the removal of the organic bpp ligand. The remaining weight is attributed to the formation of CdO (obsd, 17.89%; calcd, 20.88%) and the slow evaporation of CdO.

Photoluminescence properties

The photoluminescence properties of **1** and the H_2dtba ligand were investigated in the solid state at room temperature. As shown in Fig. 8, upon excitation at 360 nm, compound **1**

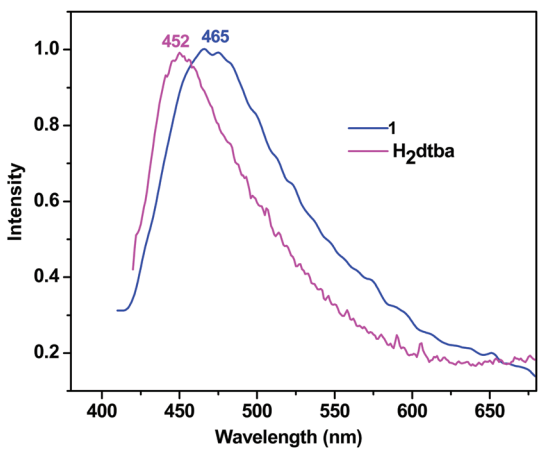

Fig. 8 Emission spectra for solid compound **1** (λ_{ex} = 360 nm) and H_2dtba (λ_{ex} = 398 nm) at room temperature.

displays a blue luminescence with a peak maximum at 465 nm. Compared with the emission spectra of H_2dtba at 452 nm (λ_{ex} = 398 nm) and bpp at 455 nm (λ_{ex} = 360 nm)[13b] red shifts of 13 nm and 10 nm in **1** were observed (Fig. 8). This may be attributed to the cooperative effect of the neutral bpp ligand and the carboxylate ligands. As a result, the emission can be assigned to intraligand fluorescence.[13b] It suggests that compound **1** might be a good photoactive material.

Photocatalytic properties

To investigate the photocatalytic activity of compound **1** as a catalyst, the photodecomposition of Rhodamine-B (RhB) in aqueous solution is evaluated under simulated sunlight irradiation. To explore the optimum conditions of photocatalytic activity, the degradation processes of RhB were studied using the same photocatalyst in different pH solutions. The different pH comparative experiments were conducted to investigate the photocatalytic activity of compound **1** under identical conditions. It is the first time that the photocatalytic activity of MOFs in different pH solutions was investigated. The pH values of RhB solution were adjusted to 1, 3, 5, 7 and 10 by adding HCl or NaOH solution.

The characteristic absorption band of RhB at 554 nm was used to monitor the degradation process as a function of irradiation time. Fig. 9 and S9–S12† show the temporal evolution of the absorption spectra of the RhB solution degraded by compound **1** at different pH values under simulated sunlight irradiation. The decomposition rate of RhB (K) can be expressed as $K = (I_0 - I_t)/I_0$, where I_0 presents the UV-vis absorption intensity of RhB at the initial time ($t = 0$) and the I_t is the intensity at a given time (t). When the pH value of the RhB solution is 1, 3, 5, 7 and 10, it is found that the maximum absorbance at 554 nm of the blank RhB aqueous solution decreases from 1.60 to 0.96, 2.00 to 1.55, 1.99 to 1.81, 2.40 to 2.22, and 2.40 to 2.23 respectively, after the 120 min simulated sunlight irradiation while those in the presence of **1** decreases from 0.93 to 0.17, 0.76 to 0.09, 1.95 to 1.70, 2.35 to 2.03, 2.38 to 1.98, respectively, at the same simulated sunlight irradiation time. On the basis of the experimental results, the decomposition rate of RhB without the catalyst and with compound **1** reach 41% and 78% at pH = 1, 23% and 85% at pH = 3, 9% and 13% at pH = 5, 7% and 13% at pH = 7, 7% and 17% at pH = 10 (120 min of simulated sunlight irradiation) (Fig. 9 and S13†), respectively. Fig. S10–S12† present the UV-vis absorption spectra of RhB at different pH values under simulated sunlight irradiation. It is found that the absorption spectra of RhB remain unchanged obviously with acidic, neutral, and basic solutions and it also means the conjugated structure of RhB does not decompose at different pH values. These results demonstrate that the use of **1** can dramatically accelerate the photodegradation reaction of RhB in aqueous solutions. These experiments also reveal that the pH values of the solution play a key role in the photodecomposition of RhB. When compound **1** was used in a pH = 3 RhB solution, the absorption peak of the dye undergoes a fairly large decrease, and the hypsochromic shifts of the absorption band are considerably insignificant (Fig. 10). It is presumed that compound **1** at pH = 3 showed the best photocatalytic activity in RhB degradation.

In addition, during the course of the photocatalytic reactions, the photostability of compound **1** was monitored using

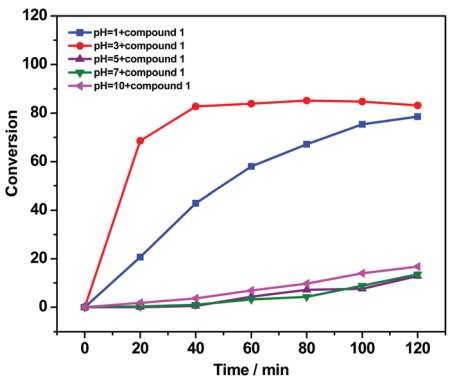

Fig. 9 Conversion rate of RhB (K) with the reaction time (t) in different pH value solutions with compound **1**.

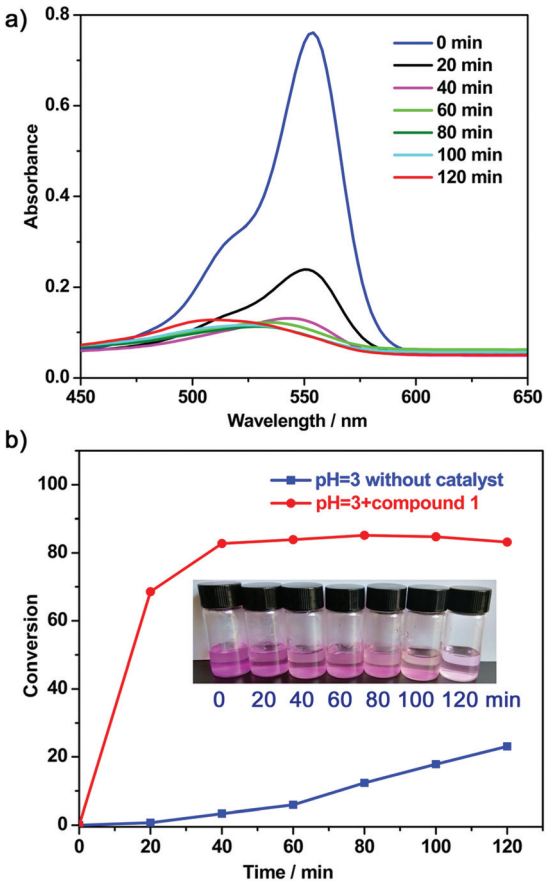

Fig. 10 (a) Absorption spectra of the RhB aqueous solution with pH = 3 during the photodegradation under 300 W high pressure Xe lamp irradiation with compound **1**; (b) conversion rate of RhB (K) with the reaction time (t) with compound **1** and without the catalyst in the pH = 3 solution.

PXRD patterns. The PXRD patterns are in good agreement with those of the original compound implying that **1** maintains its structural integrity after the photocatalysis reaction, which confirmed that its stability towards photocatalysis is good (Fig. S14†).

The possible photocatalytic mechanism[21] for the above degradation reactions is proposed as follows (Scheme S1†). Upon irradiation using simulated sunlight, the absorption of energy is equal to or greater than the band gap of **1** (Fig. S7† $h\nu \geqq 2.92$ eV), electrons (e^-) in the valence band (VB) are excited to the conduction band (CB), leaving the same amount of holes (h^+) in the VB. Electrons (e^-) have reduction and holes (h^+) have oxidation. The electrons reduce the oxygen (O_2) to an oxygen radical ($^{\bullet}O_2^-$), and finally they may turn into a hydroxyl radical ($^{\bullet}OH$) by the combination of H^+ cations. At the same time, holes oxidize the hydroxyl (H_2O) to a hydroxyl radical ($^{\bullet}OH$). Such a hydroxyl radical ($^{\bullet}OH$) is known to have high activity to decompose the organic dyes, such as RhB.[22]

$$O_2 + e \rightarrow {}^{\bullet}O_2^- + e \quad (1)$$

$$^{\bullet}O_2 + 2H^+ \rightarrow {}^{\bullet}OH + OH^- \quad (2)$$

The dissolved O_2 in an aqueous solution, as an efficient electron trap, leads to the generation of a hydroxyl radical ($^{\bullet}OH$), thus preventing the recombination of electrons and holes. According to eqn (1) and (2), the addition of HCl is favorable for the formation of a hydroxyl radical ($^{\bullet}OH$). As a result, the conversion rate of RhB is improved by the addition of an acid. Our research demonstrates that the high photocatalytic activity is achieved under acidic conditions (pH = 1 and 3), especially, compound **1** at pH = 3 showed the best photocatalytic activity in RhB degradation.

Conclusion

In summary, we have successfully constructed two 3D three-interpenetrating chiral cadmium MOF enantiomers by spontaneous resolution upon crystallization without chiral resource. Interestingly, the structure of **1** consists two types of threefold helical chiral channels (triangular and quasi-heart-like chiral channels), three types of twofold helical chiral channels (chair-like chiral channel) and one type of threefold double-helical chain. Compounds **1P** and **1M** are optically active, and their CD spectra show Cotton effects in the opposite directions. Photocatalytic activity studies reveal that compound **1** at pH = 3 shows the best photocatalytic activity in RhB degradation. It is the first time that the photocatalytic activity of MOFs in different pH solutions has been investigated.

Acknowledgements

This work was supported by the National Natural Science Foundation of China (grant 21473030 and 21003020), the Natural Science Fund of Fujian Province (grant 2013J01041) and the Foundation of State Key Laboratory of Structural Chemistry (grant 20130012).

References

1 (*a*) B. Panella, M. Hirscher, H. Putter and U. Muller, *Adv. Funct. Mater.*, 2006, **16**, 520; (*b*) D. Q. Yuan, W. G. Lu, D. Zhao and H. C. Zhou, *Adv. Mater.*, 2011, **23**, 3723; (*c*) S. Q. Ma, X. S. Wang, D. Q. Yuan and H. C. Zhou, *Angew. Chem., Int. Ed.*, 2008, **47**, 4130; (*d*) X. S. Wang, S. Q. Ma, P. M. Forster, D. Q. Yuan, J. Eckert, J. J. Lopez, B. J. Murphy, J. B. Parise and H. C. Zhou, *Angew. Chem., Int. Ed.*, 2008, **47**, 7263; (*e*) D. Yuan, D. Zhao, D. F. Sun and H. C. Zhou, *Angew. Chem., Int. Ed.*, 2010, **49**, 5357; (*f*) T. Fukushima, S. Horike, Y. Inubushi, K. Nakagawa, Y. Kubota, M. Takata and S. Kitagawa, *Angew. Chem., Int. Ed.*, 2010, **49**, 4820; (*g*) R. Vaidhyanathan, S. S. Iremonger, G. K. H. Shimizu, P. G. Boyd, S. Alavi and T. K. Woo, *Angew. Chem., Int. Ed.*, 2012, **51**, 1826; (*h*) R. B. Getman, Y. S. Bae, C. E. Wilmer and R. Q. Snurr, *Chem. Rev.*, 2012, **112**, 703; (*i*) M. P. Suh, H. J. Park, T. K. Prasad and D. W. Lim, *Chem. Rev.*, 2012, **112**, 782; (*j*) K. Sumida, D. L. Rogow, J. A. Mason, T. M. McDonald, E. D. Bloch, Z. R. Herm, T. H. Bae and J. R. Long, *Chem. Rev.*, 2012, **112**, 724.

2 (*a*) W. G. Lu, J. P. Sculley, D. Q. Yuan, R. Krishna, Z. W. Wei and H. C. Zhou, *Angew. Chem., Int. Ed.*, 2012, **51**, 7480–7484; (*b*) W. G. Lu, D. Q. Yuan, D. Zhao, C. I. Schilling, O. Plietzsch, T. Muller, S. Brase, J. Guenther, J. Blumel, R. Krishna, Z. Li and H. C. Zhou, *Chem. Mater.*, 2010, **22**, 5964.

3 (*a*) S. Q. Ma, D. F. Sun, X. S. Wang and H. C. Zhou, *Angew. Chem., Int. Ed.*, 2007, **46**, 2458; (*b*) J. R. Li, R. J. Kuppler and H. C. Zhou, *Chem. Soc. Rev.*, 2009, **38**, 1477; (*c*) M. C. Das, Q. S. Guo, Y. B. He, J. Kim, C. G. Zhao, K. L. Hong, S. C. Xiang, Z. J. Zhang, K. M. Thomas, R. Krishna and B. L. Chen, *J. Am. Chem. Soc.*, 2012, **134**, 8703; (*d*) S. Horike, K. Kishida, Y. Watanabe, Y. Inubushi, D. Umeyama, M. Sugimoto, T. Fukushima, M. Inukai and S. Kitagawa, *J. Am. Chem. Soc.*, 2012, **134**, 9852.

4 (*a*) P. F. Shi, G. Xiong, B. Zhao, Z. Y. Zhang and P. Cheng, *Chem. Commun.*, 2013, **49**, 2338; (*b*) J. J. Zhang, S. Q. Xia, T. L. Sheng, S. M. Hu, G. Leibeling, F. Meyer, X. T. Wu, S. C. Xiang and R. B. Fu, *Chem. Commun.*, 2004, 1186; (*c*) X. F. Li, Y. B. Huang and R. Cao, *Cryst. Growth Des.*, 2012, **12**, 3549; (*d*) L. Liang, G. Peng, L. Ma, L. Sun, H. Deng, H. Li and W. S. Li, *Cryst. Growth Des.*, 2012, **12**, 1151; (*e*) J. J. Zhang, S. M. Hu, S. C. Xiang, T. L. Sheng, X. T. Wu and Y. M. Li, *Inorg. Chem.*, 2006, **45**, 7173; (*f*) J. W. Cheng, S. T. Zheng, E. Ma and G. Y. Yang, *Inorg. Chem.*, 2007, **46**, 10534.

5 Y. Zhu, F. Luo, Y. M. Song, X. F. Feng, M. B. Luo, Z. W. Liao, G. M. Sun, X. Z. Tian and Z. J. Yuan, *Cryst. Growth Des.*, 2012, **12**, 2158.

6 (*a*) H. Y. Xu, F. H. Zhao, Y. X. Che and J. M. Zheng, *CrystEngComm*, 2012, **14**, 6869; (*b*) V. Chandrasekhar, B. M. Pandian, J. J. Vittal and R. Clerac, *Inorg. Chem.*, 2009, **48**, 1148; (*c*) V. Gomez, L. Vendier, M. Corbella and J. P. Costes, *Inorg. Chem.*, 2012, **51**, 6396; (*d*) Y. Liu, Z. Chen, J. Ren, X. Q. Zhao, P. Cheng and B. Zhao, *Inorg. Chem.*, 2012, **51**, 7433.

7 Q. Yue, J. Yang, G. H. Li, G. D. Li, W. Xu, J. S. Chen and S. N. Wang, *Inorg. Chem.*, 2005, **44**, 5241.

8 G. F. Xu, P. Gamez, J. K. Tang, R. Clerac, Y. N. Guo and Y. Guo, *Inorg. Chem.*, 2012, **51**, 5693.

9 (*a*) Z. Y. Li, J. Zhu, X. Q. Wang, J. Ni, J. J. Zhang, S. Q. Liu and C. Y. Duan, *Dalton Trans.*, 2013, **42**, 5711; (*b*) V. Chandrasekhar, B. M. Pandian, R. Boomishankar, A. Steiner, J. J. Vittal, A. Houri and R. Clerac, *Inorg. Chem.*, 2008, **47**, 4918; (*c*) Y. Ouyang, W. Zhang, N. Xu, G. F. Xu, D. Z. Liao, K. Yoshimura, S. P. Yan and P. Cheng, *Inorg. Chem.*, 2007, **46**, 8454; (*d*) E. Colacio, J. Ruiz, A. J. Mota, M. A. Palacios, E. Cremades, E. Ruiz, F. J. White and E. K. Brechin, *Inorg. Chem.*, 2012, **51**, 5857; (*e*) A. Jana, S. Majumder, L. Carrella, M. Nayak, T. Weyhermueller, S. Dutta, D. Schollmeyer, E. Rentschler, R. Koner and S. Mohanta, *Inorg. Chem.*, 2010, **49**, 9012.

10 (*a*) B. Zhao, X. Y. Chen, Z. Chen, W. Shi, P. Cheng, S. P. Yan and D. Z. Liao, *Chem. Commun.*, 2009, 3113; (*b*) G. Peng, G. E. Kostakis, Y. H. Lan and A. K. Powell, *Dalton Trans.*, 2013, **42**, 46; (*c*) G. M. Li, T. Akitsu, O. Sato and Y. Einaga, *J. Am. Chem. Soc.*, 2003, **125**, 12396.

11 (*a*) G. B. Deacon and R. J. Phillips, *Coord. Chem. Rev.*, 1980, **33**, 227; (*b*) K. K. Bisht and E. Suresh, *J. Am. Chem. Soc.*, 2013, **135**, 15690; (*c*) K. K. Bisht and E. Suresh, *Inorg. Chem.*, 2012, **51**, 9577; (*d*) A. Kaur, G. Hundal and M. S. Hundal, *Cryst. Growth Des.*, 2013, **13**, 3996.

12 (*a*) R. Vaidhyanathan, S. Natarajan and C. N. R. Rao, *Inorg. Chem.*, 2002, **41**, 5226; (*b*) H. Wang, Z. Chang, Y. Li, R. M. Wen and X. H. Bu, *Chem. Commun.*, 2013, **49**, 6659; (*c*) L. M. Zhang, D. Y. Deng, G. Peng, L. Sun, L. Liang, G. Q. Lan and H. Deng, *CrystEngComm*, 2012, **14**, 8083; (*d*) Z. Su, M. S. Chen, J. Fan, M. Chen, S. S. Chen, L. Luo and W. Y. Sun, *CrystEngComm*, 2012, **14**, 2040.

13 (*a*) Y. Bu, F. L. Jiang, S. Q. Zhang, J. Ma, X. J. Li and M. C. Hong, *CrystEngComm*, 2013, **13**, 6323; (*b*) R. Feng, F. L. Jiang, L. Chen, C. F. Yan, M. Y. Wu and M. C. Hong, *Chem. Commun.*, 2009, 5296; (*c*) Y. F. Hou, Y. Yu, K. F. Yue, Q. Wei, Y. L. Liu, C. S. Zhou and Y. Y. Wang, *CrystEngComm*, 2013, **15**, 7161; (*d*) M. Hu, S. T. Ma, L. Q. Guo, L. M. Zhou, L. J. Gao, S. M. Fang and C. S. Liu, *Z. Anorg. Allg. Chem.*, 2010, **636**, 616.

14 (*a*) L. H. Cao, Y. L. Wei, Y. Yang, H. Xu, S. Q. Zang, H. W. Hou and T. C. W. Mak, *Cryst. Growth Des.*, 2014, **14**, 1827; (*b*) L. Han, H. Valle and X. H. Bu, *Inorg. Chem.*, 2007, **46**, 1511; (*c*) Z. H. Li, L. P. Xue, S. H. Li, J. G. Wang, B. T. Zhao, J. Kan and W. P. Su, *CrystEngComm*, 2013, **15**, 2745; (*d*) J. C. Jin, Y. N. Zhang, Y. Y. Wang, J. Q. Liu, Z. Dong and Q. Z. Shi, *Chem. – Asian J.*, 2010, **5**, 1611.

15 (*a*) Y. Q. Zheng, J. Zhang and J. Y. Liu, *CrystEngComm*, 2010, **12**, 2740; (*b*) B. Murugesapandian and P. W. Roesky, *Inorg. Chem.*, 2011, **50**, 1698; (*c*) F. L. Hu, W. Wu, P. Liang, Y. Q. Gu, L. G. Zhu, H. Wei and J. P. Lang, *Cryst. Growth Des.*, 2013, **13**, 5050; (*d*) Q. Sun, Y. Q. Wang, A. L. Cheng, K. Wang and E. Q. Gao, *Cryst. Growth Des.*, 2012, **12**, 2234; (*e*) W. H. Zhang, Y. L. Song, Z. H. Wei, L. L. Li, Y. J. Huang, Y. Zhang and J. P. Lang, *Inorg. Chem.*, 2008, **47**, 5332.

16 (*a*) D. Sun, F. J. Liu, R.-B. Huang and L. S. Zheng, *Inorg. Chem.*, 2011, **50**, 12393–12395; (*b*) S. M. Humphrey, R. A. Mole, J. M. Rawson and P. T. Wood, *Dalton Trans.*, 2004, 1670.

17 L. Carlucci, G. Ciani, D. M. Proserpio and S. Rizzato, *CrystEngComm*, 2002, **4**, 121.

18 (*a*) Y. Q. Sun, J. Zhang, Y. M. Chen and G. Y. Yang, *Angew. Chem., Int. Ed.*, 2005, **44**, 5814; (*b*) Y. Q. Sun, J. Zhang and G. Y. Yang, *Chem. Commun.*, 2006, 1947; (*c*) Y. Q. Sun, J. Zhang and G. Y. Yang, *Chem. Commun.*, 2006, 4700.

19 (*a*) G. M. Sheldrick, *SHELXS-97, Program for X-ray Crystal Structure Solution*, University of Gottingen, Gottingen, Germany, 1997; (*b*) G. M. Sheldrick, *SHELXL-97, Program for X-ray Crystal Structure Refinement*, University of Gottingen, Gottingen, Germany, 1997.

20 (*a*) J. Li, Z. Chen, X. Wang and D. M. Proserpio, *J. Alloys Compd.*, 1997, **262–263**, 28–33; (*b*) A. Mesbah, S. Lebègue, J. M. Klingsporn, W. Stojko, R. P. Van Duyne and J. A. Ibers, *J. Solid State Chem.*, 2013, **200**, 349–353; (*c*) T.-H. Bang, S.-H. Choe, B.-N. Park, M.-S. Jin and W.-T. Kim, *Semicond. Sci. Technol.*, 1996, **11**, 1159; (*d*) Y. Q. Sun, S. Z. Ge, Q. Liu, J. C. Zhong and Y. P. Chen, *CrystEngComm*, 2013, **15**, 10188.

21 (*a*) M. C. Das, H. Xu, Z. Wang, G. Srinivas, W. Zhou, Y. F. Yue, V. N. Nesterov, G. Qian and B. Chen, *Chem. Commun.*, 2011, **47**, 11715; (*b*) T. Wen, D. X. Zhang and J. Zhang, *Inorg. Chem.*, 2013, **52**, 12; (*c*) F. Wang, Z. S. Liu, H. Yang, Y. X. Tan and J. Zhang, *Angew. Chem., Int. Ed.*, 2011, **50**, 450; (*d*) L. Liu, J. Ding, C. Huang, M. Li, H. Hou and Y. Fan, *Cryst. Growth Des.*, 2014, **14**, 3035.

22 (*a*) C. Galindo, P. Jacques and A. Kalt, *J. Photochem. Photobiol., A*, 2000, **130**, 35; (*b*) J. Joseph, H. Destaillats, H. Hung and M. Hoffmann, *J. Phys. Chem. A*, 2000, **104**, 301–307.